Nuclear Engineering and Technology 54 (2022) 1049–1061

Contents lists available at ScienceDirect

Nuclear Engineering and Technology

journal homepage: www.elsevier.com/locate/net

Original article

Gamma and neutron shielding properties of B_4C particle reinforced Inconel 718 composites

Uğur Gökmen

Gazi University, Faculty of Technology, Department of Metallurgical and Materials Engineering, 06500, Ankara, Turkey

ARTICLE INFO

Article history:
Received 16 March 2021
Received in revised form
23 August 2021
Accepted 19 September 2021
Available online 27 September 2021

Keywords:
Inconel 718
Superalloy
B_4C
Radiation attenuation properties
Neutron removal cross-section

ABSTRACT

Neutron and gamma-ray shielding properties of Inconel 718 reinforced B_4C (0-25 wt%) were investigated using PSD software. Mean free path (MFP), linear and mass attenuation coefficients (LAC,MAC), tenth-value and half-value layers (TVL,HVL), effective atomic number (Z_{eff}), exposure buildup factors (EBF), and fast neutron removal cross-sections (FNRC) values were calculated for 0.015–15 MeV. It was found that MAC and LAC increased with the decrease in the content of B_4C compound by weight in Inconel 718. The EBFs were computed using G-P fitting method for 0.015–15 MeV up to the penetration depth of 40 mfp. HVL, TVL, and FNRC values were found to range between 0.018 cm and 3.6 cm, between 2.46 cm and 12.087 cm, and between 0.159 cm^{-1} and 0.194 cm^{-1}, respectively. While Inconel 718 provides the maximum photon shielding property since it offered the highest values of MAC and Z_{eff} and the lowest value of HVL, Inconel 718 with B_4C(25 wt%) was observed to provide the best shielding material for neutron since it offered the highest FNRC value. The study is original in terms of several aspects; moreover, the results of the study may be used in nuclear technology, as well as other technologies including nano and space technologies.

1. Introduction

Despite increasing nuclear applications in various fields, nuclear radiation has played a critical role in recent years. The radiation applications have been successfully used in industry, medicine, research and development studies, and agriculture. The gamma-ray and neutron sources are not only sensitive laboratory equipment but also hazardous for human health. Therefore, life and radiation cannot be separated because radiation is inevitable in our daily life. Accordingly, radiological measurements and radiation protection are significant subjects for nuclear studies particularly for accelerators, nuclear power plants, detector manufacturers, and other widespread use of radioactive isotopes in several fields [1–4]. Radiation shielding is required for the protection from the hazardous effects of gamma-rays and penetrative neutrons. The following three factors change the intensity of penetrating radiation of neutrons and gamma-rays: distance, shielding, and time. The shielding, which is implemented naturally or by utilizing composite materials, has been widely and effectively used for protection from hazards of radiation. The interactions between the radiation and the atoms in the shielding material provide an advantage in decreasing the radiation effect. Passive shielding should be designed to provide a durable and non-toxic solution with less secondary radiations. It should also offer multiple functions, convenience, cost-effectiveness, as well as effective protection [4–6].

Recently, novel multifunctional composites have been studied to improve gamma-ray shielding materials. Due to the widespread use of gamma-ray's active isotopes in agriculture, industry, and medicine, researching the interaction and absorption of gamma radiation in materialsis important. The atomic, electronic, and molecular cross-sections, mass energy-absorption coefficient (MAC), electron density, effective atomic number, mean free path (MFP), exposure buildup factor (EBF), energy absorption buildup factor (EABF), and the tenth-value and half-value layer (TVL, HVL) thicknesses of the materials are important and useful parameters to understand their physical properties in terms of their shielding effectiveness [6–8].

All or some of these parameters were determined for alloys [5–7], minerals [8,9], gemstones [10,11], polymers [12], amino acids [13], semiconductors [14], superconductors [15], glasses [16–19], and building materials [20–22] in the last decade. Moreover, several researchers tried to determine these parameters by applying various methods [23,24]. According to the results of these

E-mail address: ugurgokmen@gazi.edu.tr.

https://doi.org/10.1016/j.net.2021.09.028

studies, the radiation shielding materials were frequently found to have a significant effect on the protection of human life and other materials from their degrading effects. As it is well known, the harmful radiations emitted by unshielded radioactive sources have degrading effects on human life and other materials. The radiation shielding materials decrease the dangerous radiation dosage by direct interaction with radiation, thereby reducing the radiation energy.

According to Lamber–Beer law$I = I_0 e^{-\mu x}$, where$I$denotes the transmitted intensity, I_0 denotesthe incident intensity, μdenotes the linear attenuation coefficient (LAC), and $x$denotes the thickness of the shielding material, gamma rays collimated into a narrow beam are decreased by a shield. Depending on the physical state of the material, the absorber density is proportional to linear attenuation coefficients. In case each condition is not met, this law cannot beused. The law can only be used by utilizing a correction factor, i.e. the "buildup factor". The buildup can be defined as the ratio of the total value of the specified radiation at any point to the contribution of the radiation to that value by reaching the point without undergoing a collision. It is a significant quantity for estimating the distribution of photon flux in the irradiated medium. Several computer codes including ADJMON-I [25,26], PALLAS [27], and EGS4 [28] can be used to compute buildup factors. Two types of buildup factors are computed: (a) EBF and (b) EABF [29,30]. While the values of these factors are computed using various methods, the G-P fitting method provides the most appropriate value [31]. American National Standards ANSI/ANS 6.4.3 [32] provides the buildup factors of 23 elements with atomic numbers (Z) ranging between 4 and 92 by using the G-P method covering the energy range 0.015–15 MeV up to penetration depth of 40 mfp. Several researchers studied the EBF and EABF for various mixtures, compounds, composites, amino acids, and carbohydrates [33], polymers [34], concretes [35], bismuth borosilicate glasses [36], superconductors [37], and solvents [38]. These studies indicate the convenience of the G-P method in computing both buildup factors, EBF and EABF.

High-density materials such as metals, concrete, metal alloys, lead bricks, and multiple layers of single slabs of pure elements (Pb, Al, Cu, Fe, Mo) are used for radiation shielding [39]. The type and activity of radiation, its dose rate, and the source material which is satisfactory for the externalshielding determine the required type and amount of shielding. Owing to their outstanding internal properties, superalloys perform well at high temperatures. Superalloys, which are based on nickel, cobalt, or iron, show suitable oxidation resistance, superior strength at high temperatures, and high heat corrosion resistance. As high-temperature alloys, nickel-based alloys are the most widely used ones. Consequently, nickel-based alloys are frequently used in the aerospace, marine, power generation turbine components, petrochemical, nuclear reactor, and pollution control equipment industry [40–43]. Nickel-basedsuperalloys are the major materials preferred for high-temperature applications in aircraft and power systems. These alloys are effectively used because of their stability at high temperatures as well as their extreme resistance to corrosion [44]. The chromium and molybdenum content in the alloy providesa significant increase in the corrosion resistance property [45]. The strength of nickel-based alloys can be improved by using the solid solution strengthening method or by hardening them through intermetallic compound precipitation in the face cubic center (fcc) matrix. Inconel 718 is also a typical nickel-based superalloy. Nickel-based superalloys of Inconel 625 and Inconel 601 are derivatives of the Inconel 718 alloy. As a special series of nickel-based superalloys, Inconel alloys differ from others in terms of the weight of alloying elements content. In their study, ZelinXu et al. reported that the increase in the amount of B_4C content in the Inconel 625 alloy increased its hardness and wear resistance [46].

Due to its superior strength at high temperatures and high heat corrosion resistance, Inconel 718 has been widely used as a superalloy in various applications. Inconel 718 is widely used in the rocket components, aircraft, gas turbines, and nuclear reactors industry since it offers microstructural stability, high corrosion resistance, and high strength up to the temperature of 650 °C. As a nickel-chromium alloy, Inconel 718 has significant contents of iron, niobium, and molybdenum, and it can be hardened by γ'' precipitation. Since the density of Inconel 718 superalloy is very, it can be used as a gamma-ray shielding material [47].

Therefore, studying the features of Inconel 718 in detailis exciting. In recent years, Inconel 718 and its composites have been developed, and the powder metal parts were performed by the powder metallurgy method [48]. Many types of particle reinforced composites are used in industrial applications. Several types of ceramic materials, SiC, and B_4C are widely used to reinforce metal alloy matrixes [49,50]. In the literature, many studies have examined various shielding materials manufactured by adding B and B compounds into various materials [51]. The B_4C compound is an ideal addition for the neutron and gamma-ray radiation shielding materials due to their high hardness, good melting point, good modulus, impact properties, and good tribological properties, as well as good chemical resistance [50–53]. The concentration of elemental boron in B_4C is 85%. Natural boron is known to contain 19.8% high-cross-section isotope. On the other hand, natural B_4C contains 14.7%^{10}B in its content. While the thermal neutron absorption cross-section of ^{10}B is 3840 b, this value is about 600 b for the natural B_4C [53,54]. Because the absorption cross-section of boron is high, these materials can absorb gamma rays, thermal neutrons, and fast neutrons effectively, thereby, enabling the material as a neutron absorber for dry caskstorages, as well as wet storage pools [53,54]. Numerous studies concentrated on the B_4C content of the shielding material to confirm its suitability for nuclear shielding applications.The increase in the B_4C content was reported to cause an increase in the neutron and gamma-ray shielding capacity of the material [55–57].

The present study aims to research the gamma-ray and neutron attenuation behaviors of a novel shielding material of Inconel 718 superalloy containing B_4C (0–25 wt%) particle using the Phy-X platform. These composite materials'shielding effectiveness for gamma-ray and neutron has not been studied until now. In this study, the LAC, MAC,TVL, HVL, MFP,and EBF, Z_{eff}, and FNRC values of the B_4C (0–25 wt%) particle-reinforced Inconel 718 superalloy composites were theoretically calculated considering the radiation shielding for the first time. Moreover, the EBFs values were computed for the photon energy ranging between 0.015 MeV and 15 MeV up to penetration depths of 40 mfp using the G-P fitting method. Furthermore, all the values calculated for these composite materials by running the Phy-X platform were compared with each other.

2. Materials and computational method

2.1. Materials

Inconel 718 superalloy powder and reinforced B_4C (5 wt%, 10 wt %, 15 wt%, 20 wt%, 25 wt%) powder were utilized as the starting material for the theoretical calculation of Inconel 718 matrix composites. Inconel 718 superalloy powders used in studies were obtained from Sandvik Osprey Limited (United Kingdom).Gasatomized Inconel 718 was used as matrix metal powder in the present study. While the pycnometer densityof gas atomized Inconel 718 was 8.20 g/cm^3, the pycnometer density of B_4C powder was 2.52 g/cm^3. Matrix powder particles, which usually havea

spherical form, are shown in Fig. 1. The chemical composition of the Inconel 718 superalloy powder used in the study is given in Table 1. Fig. 2 presents the energy-dispersive X-ray (EDX) spectroscopy analysis of Inconel 718 powders. Fig. 3 presents the size distribution of the powders, which was determined using alight particle sizing system (Malvern Panalytical Mastersizer 3000-E). Inconel 718 powder with an average size of about ~9.68 μm at D10, ~24.92 μm at D50, and ~50.68 μm at D90 were produced by gas atomization. The B_4C particle, which has an average size of about ~4.60 μm at D50, ~2.65 μm at D10, and ~8.25 μm at D90, was used as reinforcement material. EDX analyses and SEM images of Inconel 718 powder indicated that the present study may form a basis for new experimental studies. The study will provide the needed insight to compare the results of the further experimental studies using composite samples that will be produced using Inconel 718 powder with spherical form.

According to the rule of mixture, theoretical densities of composites were calculated as follows: Inconel 718 reinforced B_4C (5 wt %),7.91 g/cm^3 (density); Inconel 718 reinforced B_4C (10 wt%), 7.63 g/cm^3 (density); Inconel 718 reinforced B_4C(15 wt%), 7.34 g/cm^3 (density), Inconel 718 reinforced B_4C (20 wt%), 7.06 g/cm^3 (density); Inconel 718 reinforced B_4C (25 wt%),6.78 g/cm^3 (density). Inconel 718, Inconel 718 reinforced B_4C (5 wt%), Inconel 718 reinforced B_4C (10 wt%), Inconel 718 reinforced B_4C(15 wt%), Inconel 718 reinforced B_4C (20 wt%), and Inconel 718 reinforced B_4C (25 wt%) were defined as S1, S2, S3, S4, S5, and S6, respectively.

2.2. Computational method

2.2.1. Mean free path,tenth-value layer,and half-value layer

In terms of its energy,the radiation could be described as non-ionizing and ionizing. There are two principal types of ionizing radiations:directly ionizing radiations and indirectly ionizing radiations. Radiations of energetic particles carrying an electric charge, such as beta particles, alpha particles, protons, and other recoil nuclei comprise the directly ionizing radiations. Direct action of these radiations on electrons of atoms of the media through which they pass causes ionization. On the other hand, indirectly ionizing radiations, such as x-ray or gamma-ray photons and neutrons, are not charged. These radiations provide ionization by a more complicated mechanism where energetic secondary charged particles are emitted tocause most of the ionization.

Since heavy ions may interact with nuclei, they mayslow down in the medium. The incident ion may be fragmented during these interactions. This fragmentation depends on the characteristics of the medium, the type of the ion, and its energy. Usually, the initial velocity of these fragments is about the same as the velocity of the primary ions, they have a smaller nuclear charge. Since the rate of energy loss varies depending on the square of the nuclear charge, they offer a lower rate of energy loss compared to the primary ion. Therefore, the variation in the energy loss, as well as the ranges of the particles are large. The effect of fragmentation on the absorbed dose distribution in linear energy transfer determines the significance of primary beam ions'fragmentation. An absorber nucleus may also be subjected to fragmentation due to inelastic interactions. The energies of the charged fragments resulting from a target nucleus fragmentation will be lower than those of the fragments resulting from a projectile. Therefore, the dose caused by the target fragments is usually deposited locally [57–59].

The interaction between the directly ionizing radiation and shielding media is very strong; therefore, it can be stopped easily. On the other hand, indirectly ionizing radiation may penetrate very easily; therefore, massive and expensive shielding may be required. Because of these reasons, the shielding of neutrons and photons, which are the most frequently encountered types of indirectly ionizing radiation, attracts attention today [57–59].

When a gamma-ray with an energy of 10,000 times greater than that of the visible photons ray interacts with the matter, the main processes of photoelectric absorption, pair production, and Compton scattering (CS) are observed. On the other hand, when the gamma rays with low energy interact with matter, it causes a photoelectric effect leading to the emission of photoelectrons. Also, the gamma rays with intermediate energy lead to an increase in the Compton scattering phenomenon. In most absorbing materials, the cross-sections of photoelectric interactions are sufficiently high, and their energies are lower than 500 keV. Moreover, the cross-sections of the CS are important for the energies ranging between 100 keV and 10 MeV, and the pair-production process becomes significant for the energies above 2 MeV [57–59].

Depending on the physical state, the absorber density of the material is proportional to linear attenuation coefficients. However, usually, the MAC is used for eliminating the density dependence. Thus, MAC values (cm^2/gr) of alloys are defined as follows:

$$\frac{\mu}{\rho} = \sum_i w_i \left(\frac{\mu}{\rho}\right)_i \tag{1}$$

whereρ,μ, and w_i denote the sample density, linear attenuation coefficient (LAC), and the weight fraction, respectively [59].$\mu$is dependent on the incident gamma-ray energy and Z of the elements of the medium.

Shielding materials'HVL, TVL, and MFP properties are required to calculate the strength of gamma-ray shielding. HVL and TVL are thicknesses of the sample that will decrease the intensity of the primary photon beam in the order of half and tenth. These values can be computed as follows [60]:

$$HVL = \frac{\ln 2}{\mu} \tag{2}$$

$$TVL = \frac{\ln 10}{\mu} \tag{3}$$

$$MFP(cm) = \frac{1}{\mu} \tag{4}$$

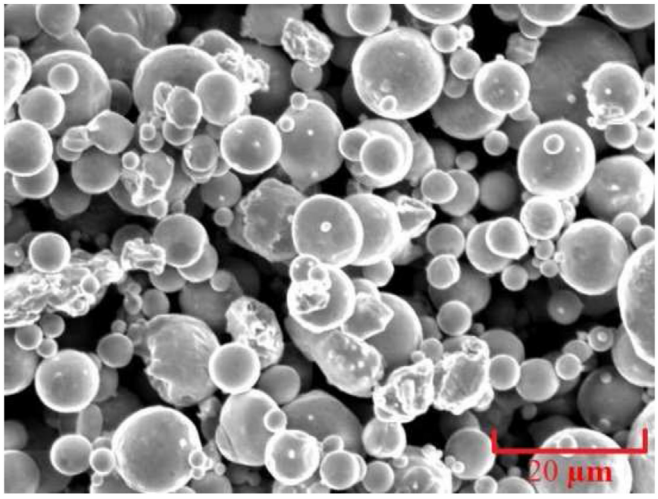

Fig. 1. SEM image of Inconel 718 powders with spherical form.

Table 1
Chemical composition of Inconel 718 powders.

Powder		C	Mn	Si	B	Cr	Mo	Ni	Nb	Cu	Al	Ti	Fe
Inconel 718	**Min.**	0.03	–	–	–	17.0	2.8	50	4.75	–	0.2	0.65	M
	Max.	0.06	0.12	0.22	0.006	21.0	3.3	55	5.50	0.3	0.8	1.15	M

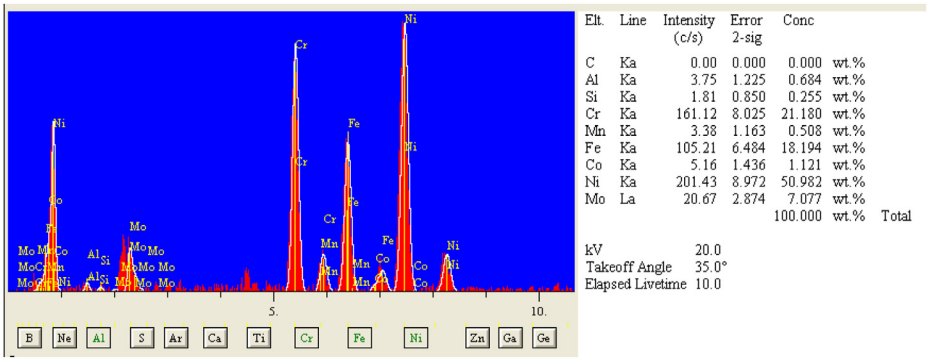

Fig. 2. Results of the EDX analysis of the Inconel 718 powders.

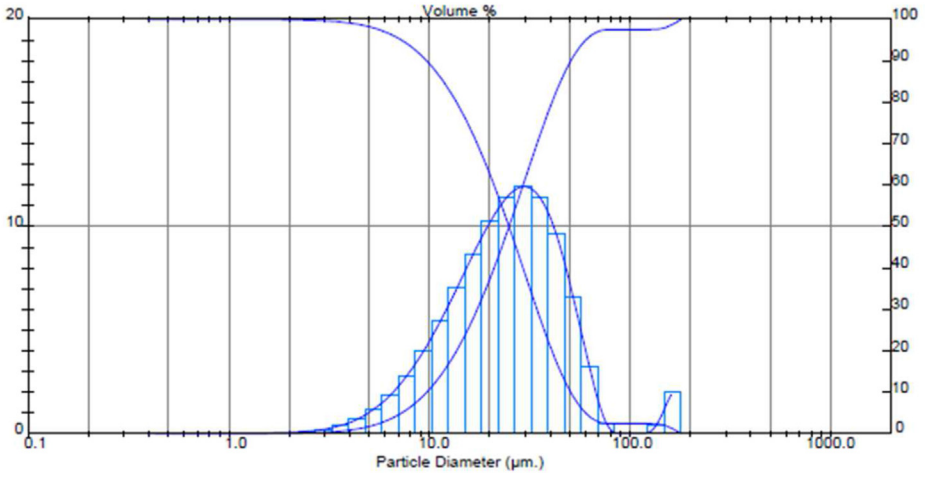

Fig. 3. Particle size distribution plot of the Inconel 718 powders.

2.2.2. Exposure buildup factors

The buildup factors can be calculated using the Geometric Progression (G-P) fitting method. The studied composite materials' (S1–S6) gamma-ray exposure buildup factors were also calculated using the Geometrical Progression equation. It is well known that this equation accurately gives the buildup factors of various materials in a wide energy range and thickness [34,60–64].

The G-P fitting parameters and EBFs of the studied composites were computed using the interpolation method. These parameters were computed in the following three stages as.

(a) Computing Z_{eq}
(b) Computing G-P fitting parameters
(c) computing EBF and EABF.

Gamma-ray's interaction with them edium, pair-production, Compton scattering, photoelectric, and absorption dependson energy and Z. Thus, Z_{eq} varies concerning the photon energy for each interaction. However, the photons buildup in the medium mainly because of the multiple scattering events by Compton scattering. Therefore, only the Compton scattering interaction process could be used to obtain the Z_{eq}values of the studied composites. The Z_{eq} value was predicted using the ratio of$(\mu/\rho)_{Compton}/(\mu/\rho)_{Total}$ at a specific energy level with the corresponding element at the same energy. In this way, the values of $(\mu/\rho)_{Compton}$and $(\mu/\rho)_{Total}$were calculated using WinXCom for the elements with Z between 4 and 40 in the energy region ranging between 0.015 and 15 MeV [61,62]. The value of Z_{eq} was calculated using the equations in the interpolation method [63]. Similarly, the G-P fitting parameters were also calculated. The G-P fitting parameters of the elements were received from the database of the ANS-6.4.3 standard. Also, the EBF values were predicted using the G-P fitting parameters (b,c, a, X_k, and d) in the gamma-ray energy range between 0.015 and 15 MeV up to 40 mfp using the following equations [63];

$$B(E,X) = 1 + \frac{b-1}{K-1}(K^x - 1) \quad for \quad K \neq 1 \tag{5}$$

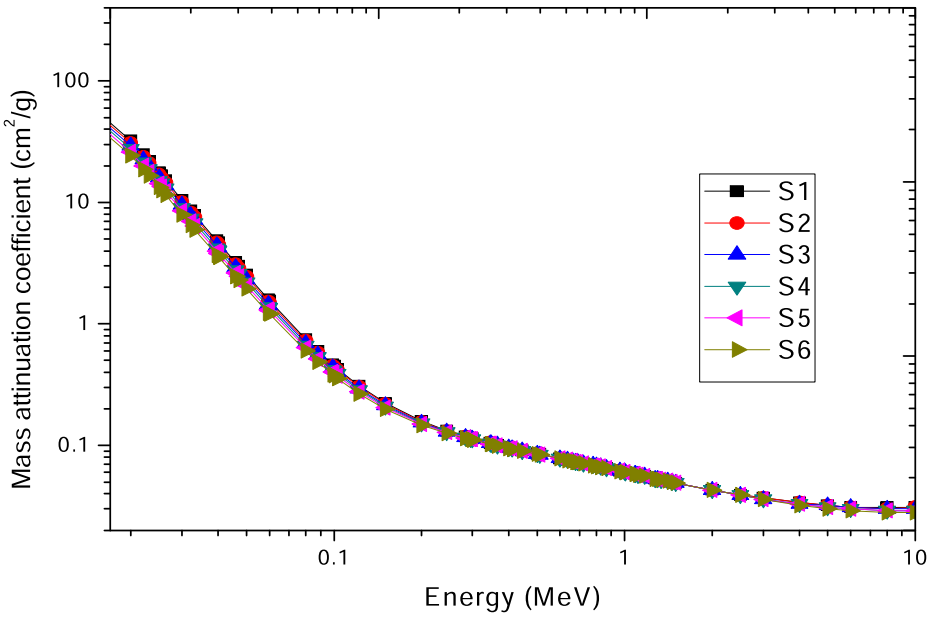

Fig. 4. The plot of the mass attenuation coefficients (MAC) versus the gamma-ray energy.

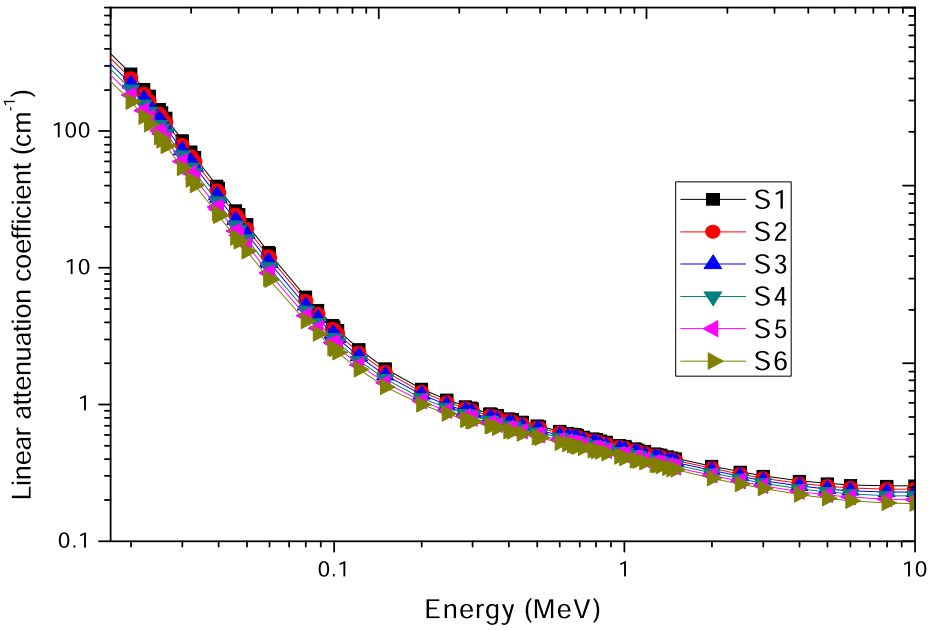

Fig. 5. The plot of the linear attenuation coefficients (LAC) versus the gamma-ray energy.

$$B(E,X) = 1 + (b-1)X \quad for \quad K = 1 \tag{6}$$

$$K(E,X) = cX^{a} + d\frac{\tanh(X/X_K - 2) - \tanh(-2)}{1 - \tanh(-2)} \tag{7}$$

for the penetration depth of $(X) \leq 40$ mfp.where $K(E, X)$denotes the dose multiplicative factor, Xdenotes the source-detector distance for the medium in terms of mfp, b denotes the value of EBF at 1 mfp, and$b$,c,a,X_K, and $d$denote the calculated G-P fitting parameters [64].

2.2.3. Fast neutron removal cross-section (FNRCS)

Neutrons have been widely used in several fields of medicine including radiotherapy, radiobiological research, nuclear medicine, boron neutron capture therapy (BNCT), as well as nuclear reactors, particle accelerators, and industry. Although the neutrons do not cause direct ionizing radiation, they directly enter the nuclei of substances. Thus, they show indirect ionizing radiation characteristics [65]. Because of this behavior of neutrons, studies on neutron shielding are quite important. Because neutrons are particles without charge, they can interact with a medium through various mechanisms. such as inelastic and elastic scattering, neutron capture, nuclear fission, and nuclear spallation. The fast neutron removal cross-section$\sum_{\sum_R}$ is a common parameter to compute the potentiality. It is defined as follows:

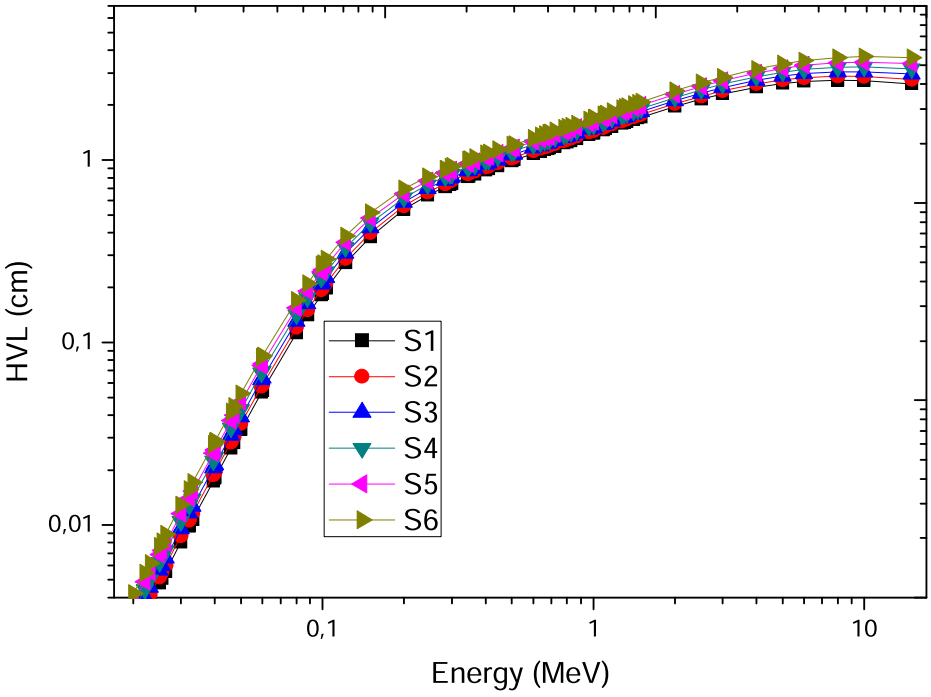

Fig. 6. The plot of the HVL versus the gamma-ray energy.

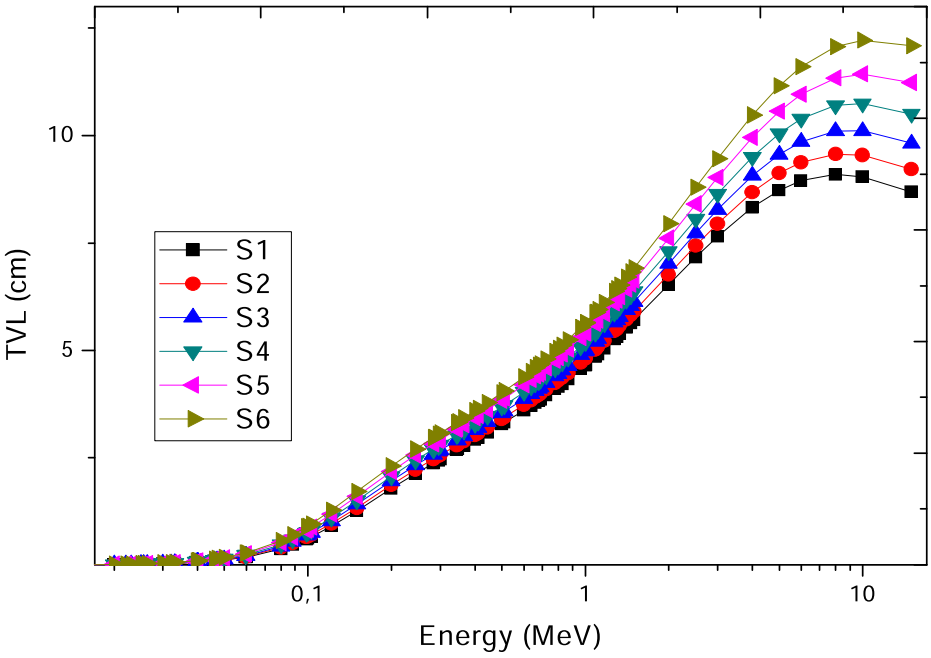

Fig. 7. The plot of the TVL versus the gamma-ray energy.

$$\sum_R = \sum_i \rho_i \left(\sum_R / \rho \right)_i \tag{8}$$

where, $(\sum_R/\rho)_i$ and ρ_i denote mass removal cross-section and the partial density of the ith constituent, respectively. The mass removal cross-section values of the elements were adopted from Chilton and Kaplan [66,67].

3. Results and discussion

3.1. Linear and mass attenuation coefficients(LAC, MAC)

MAC values of the S1–S6 composites versus the energy of gamma rays are calculated for the energy levels between the 13,8 keV and 15 MeV by using the Phy-X application. The Phy-X/PSD is an online application thatruns on are mote server. The configuration details of this remote server with the Ubuntu 14.04.3 LTS operating system are as follows: Intel(R) Core(TM) i7-2600 CPU

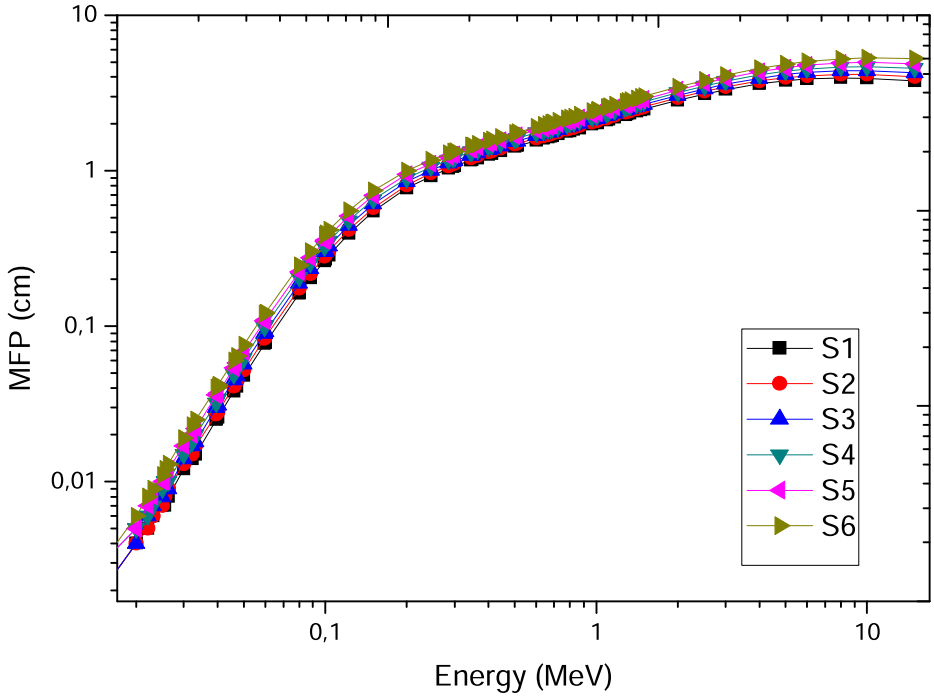

Fig. 8. The plot of the MFP versus the gamma-ray energy.

@ 3.40 GHz,1 GB installed memory. The programming language of the application is NodeJS v8.4.0 serving with Nginx 1.15.8. A secure 256 Bit Positive SSLencryptionis used between the client and server to ensure security [64]. The users need to access the https://phy-x.net/PSD address to be able to run the PSD software. The Geometric Progression (G-P) fitting method is offered to compute the buildup factors.

Fig. 4 shows the MAC versus gamma energy by the weight fractions of the B_4C compound in Inconel 718 superalloy matrix composite materials. According to the figure, MAC values decrease sharply for all the studied composites (S1–S6). Also, the total mass attenuation coefficient (μ/ρ), which depends on the energy applied, decreases with the increase in the weight fraction of the B_4C compound in the Inconel 718 superalloy matrix composite. This coefficient also decreases with an increase in gamma-ray energy, which ranges between 13.8 keV and 15 MeV, owing to the different densities and chemical composition of these materials. The values of (μ/ρ) are observed to be higher in low-energy regions while they decrease until 1.5 MeV for the S1– S6 matrix composites. On the other hand, the MAC values are observed to decrease slightly after 1.5 MeV; then, they seem stable below 4 MeV. The photoelectric effect is a dominant factor for low-level energy, and the cross-section of the photoelectric effect proportionally changes with Z^{4-5}. On the other hand, the pair production process is the dominant factor for high-level energy, and the cross-section of this process is related to Z^2. The significance of Compton scattering increases after 0.3 MeV since MAC values reduce more slowly compared to the increase in the photon energy. This can be attributed to the prevalence of Compton scattering at medium energies and the change in the cross-section of the photon-sample interaction with Z/E in the medium-level energy regions [68]. It reveals that the density is important in terms of affecting both MAC values of the photon energy and variations in the chemical composition of the materials. As a result, the computed values of the total mass attenuation coefficients imply that a decrease in the weight fraction of the B_4C compound in Inconel 718 superalloy matrix composites leads to better attenuation performance as a gamma shielding material.

Fig. 5 shows the LAC versus gamma energy by the weight fractions of B_4C compound in the Inconel 718 superalloy matrix composites. Similar to MAC values, the LAC values also decrease with the increase in the weight fraction of the B_4C compound in the Inconel 718 superalloy matrix composites, thereby making it an undesirable material for radiation shielding. This is because the B_4C compound's atomic number (Z) is lower than that of the Inconel 718 superalloy. The attenuation of the gamma-ray gets higher in line with the higher figures of Z values of the materials.

3.2. Tenth-value and half-value layers (TVL,HVL)

As seen in Fig. 6 and Fig. 7, the HVL and TVL values for various gamma rays increase with the increase in the weight percentage of the B_4C content in the Inconel 718 superalloy matrix composites. This is attributed to the different densities and chemical compositions of the Inconel 718 superalloy matrix composites with various weight fractions of the B_4C compound. As can be seen, HVL and TVL decrease with the decrease in the photon energy, and they become stable after 10 MeV for the S1–S6 matrix composites. The HVL and TVL values show a significant change in the energy range between 0.013 MeV and 10 MeV depending on the chemical composition. The HVL values of the S1–S6 matrix composites are observed to range between 0.018 cm and 0.9 cm at the low-energy region (0.013 MeV < E < 0.3 MeV). On the other hand, these values are observed to range between 0.9 cm and 3.6 cm at the high-energy region (0.3 MeV < E < 10 MeV). Also, the range of the TVL values of these composites is between 0.004 cm an2.46 cm for the low-energy region (0.013 MeV < E < 0.3 MeV), while it is between 2.46 cm and 12.087 cm for the high-energy region (0.3 MeV < E < 10 MeV). Moreover, the HVL and TVL values change inversely proportional to the density of these materials. Composites with lower HVL and TVL values show higher shielding against gamma-ray photons. Since Inconel 718 superalloy has the minimum HVL and TVL values, it provides an excellent shielding ability

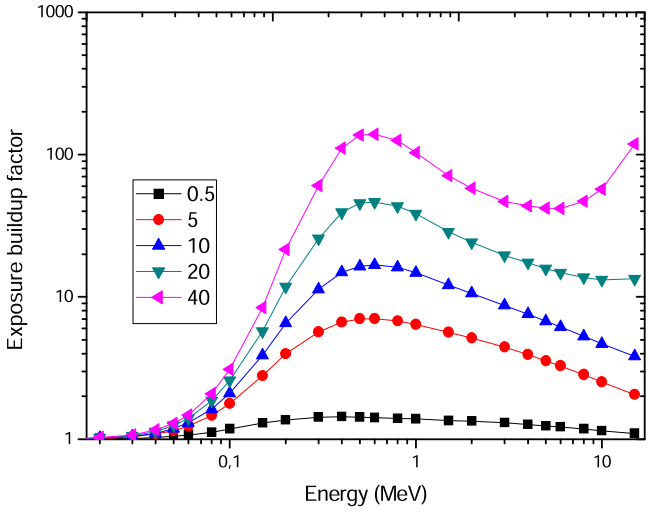

(a)

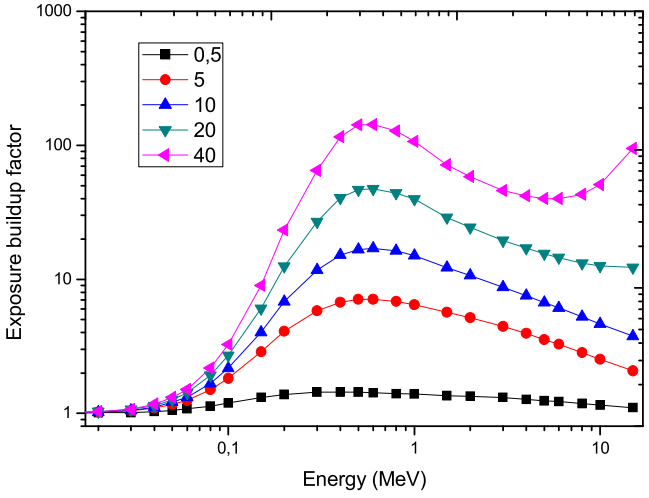

(b)

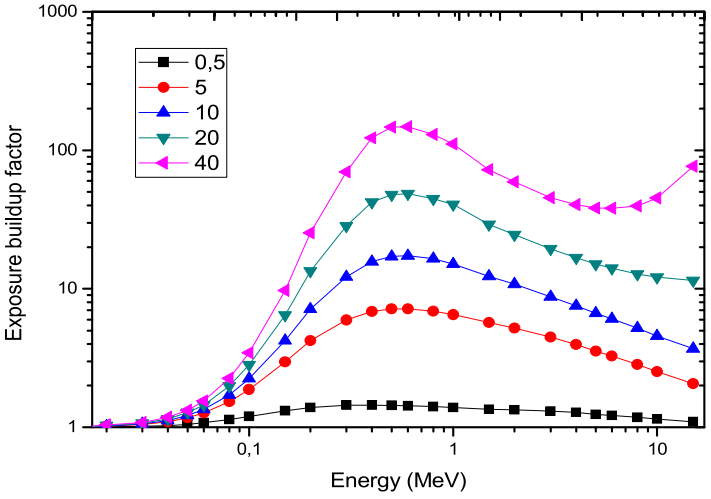

(c)

Fig.9. (a–f) The variation of the exposure buildup factor of matrix composite materials (S1–S6) with photon energy for 0.5 mfp, 5 mfp, 10 mfp, 20 mfp, and 40 mfp.

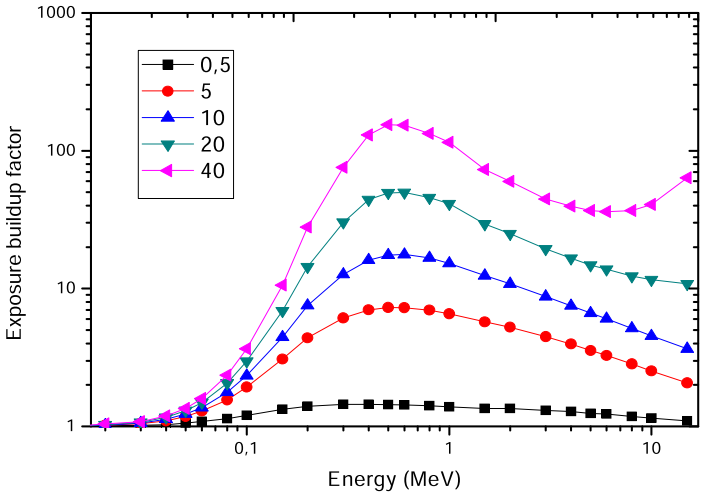
Exposure buildup factor
Energy (MeV)
0,5
5
10
20
40
1000
100
10
1
0,1
1
10

(d)

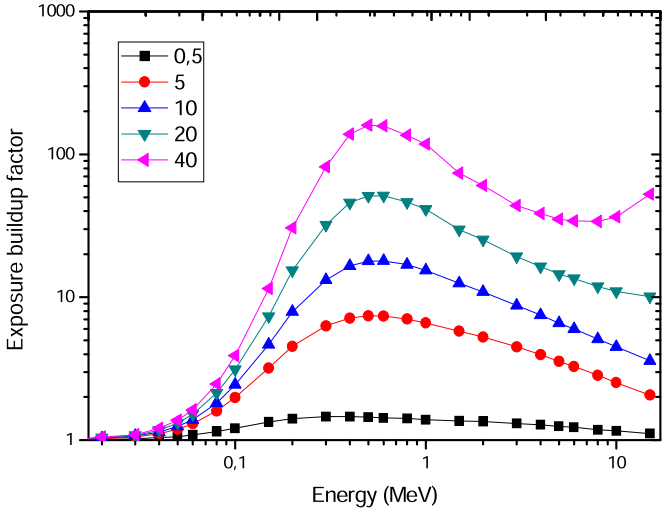
Exposure buildup factor
Energy (MeV)
0,5
5
10
20
40
1000
100
10
1
0,1
1
10

(e)

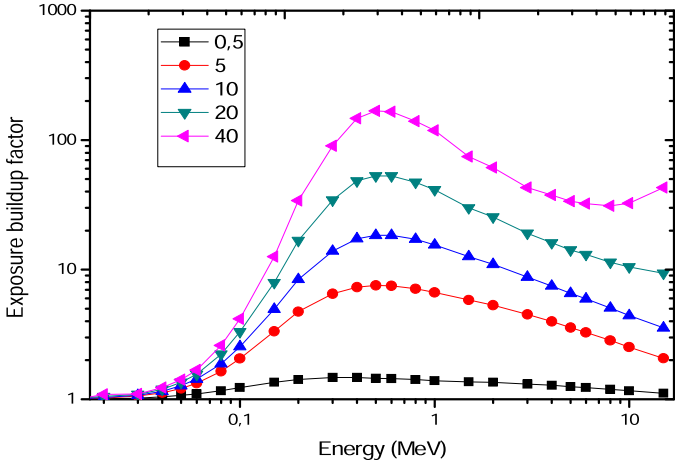
Exposure buildup factor
Energy (MeV)
0,5
5
10
20
40
1000
100
10
1
0,1
1
10

(f)

against gamma radiation. Consequently, because Inconel 718 superalloys with B_4C addition have a low gamma absorption cross-section, these materials cannot absorb a wide range of gamma rays effectively.

3.3. Mean free path (MFP)

Fig. 8 presents the MFP values and the gamma-ray energy of the S1–S6 composites. The figure reveals that the thickness of the S6 composite should be higher compared to other composites for all energy regions. Since the S1 composite shows the minimum MFP values, it can be interpreted that it provides the best shielding compared to others. As already stated, the MFP value of the alloys changes depending on the density and the Z value of the elemental composition. Fig. 8 reveals that MFP values decrease with the decrease in the photon energy and become stable after 10 MeV similar to HVL and TVL. The MFP value shows a significant change depending on the chemical composition.

3.4. Exposure buildup factors

Fig. 9(a–f) shows the variation of the EBFs by the gamma-ray energy considering the weight fraction of the B_4C compound in the Inconel 718 superalloy matrix composites for a penetration depth between 0.5 and 40 mfp. The figure reveals that the increase in the penetration depth of the materials results in an increase in the thickness of the interacting medium.As a result, the scattering events in the interacting medium increases, particularly for the material with the highest equivalent atomic number. Thus, it causes larger EBF values. The variation of the EBFs can be attributed to the interaction cross-section which depends on the photon energy and the Z of the elements. Accordingly, the S1 composite has the highest EBF values, the S6 composite has the lowest EBF values. The S1–S6 composites have lower EBF values in the low and high photon energy regions. The EBF values have a peak at 0.6 MeV for the S2–S6 composites and at 0.4 MeV for the S1 composite in the intermediate energy region due to a very high rate of multiple scattering. The photons may lose most of their energy or completely disappear at low energies dominated by the photoelectric effect process [69]. Since most photons are absorbed by the sample in this region, the EBF values get lower. Since the Compton Scattering process is dominant after the energy level of 0.1 MeV, other scatterings begin to increase. Photons leave the sample strongly or lose little energy due to secondary scatterings. Therefore, the EBF values get their highest values in all series. Fig. 9(a–f) also reveals that the EBF values begin to decrease again after the energy level of 1 MeV. This can be attributed to the pair production (PP) process which is effective in higher energy levels. Similar to the PE, the photons also lose their energy or disappear completely in the PP process. Sometimes, secondary scattering and photon buildup may be observed depending on the sample content. Usually, the EBF values are observed to reduce in the higher energy regions in all samples. Also, the pair production phenomenon is observed to dominate the Compton effect for energies higher than 10 MeV. This phenomenon results in lower values of the buildup factor at this energy region for the S1–S6 composites because of the absorption behavior of this process. Moreover, the EBF values are observed to increase with the increase in the depth of penetration. This is an expected result since the photons strengthen each other in case of an increase in the thickness of the material.

Fig. 10 shows the variation of the effective atomic numbers (Z_{eff}) in the S1–S6 composites due to different photon energies. The Z_{eff} value is very sensitive to variations in these composite materials. The Z_{eff} value decreases when the energy gets higher due to the CS phenomena. The increase in the gamma energy and weight fraction of the B_4C compound in the Inconel 718 superalloy matrix composites decreases the Z_{eff} values. With the increase in the photon energy, the Z_{eff} value is observed to reduce at the beginning, then becomes stable, and finally increases. It can be concluded that the materials have higher Z_{eff} values in photoelectric effect regions and pair production regions while they have the lowest Z_{eff} values in the Compton effect region. It can be summarized that the S1 composite, which has the highest μ/ρ and Z_{eff} values and the lowest HVL value, provides the best photon shielding compared to other matrix composites.

The results of the analyses indicate that the Inconel 718 superalloy matrix composites absorb a wide range of gamma-rays effectively. Since shielding material and its thickness are decided depending on the incident gamma-ray energy, this study suggests that each quantity depends on the energy.

3.5. Fast neutron removal cross-section (FNRC)

In neutron shielding studies, the effective neutron removal cross-section ΣR (cm^{-1}) is a significant parameter, and higher values of it indicate better shielding capacity [65]. Table 2 presents the FNRC values of the S1–S6 composites. The S6 composite was found to have the highest removal cross-section because its Z_{eff} value and density are low. The FNRC values also reveal the neutron shielding effectiveness of the studied Inconel 718 superalloy matrix composites with B_4C addition. Therefore, it can be concluded that lower values of Z_{eff} elemental composition and density have a key role in better neutron shielding.

4. Conclusion

The present study aimed to provide a computational tool that would perform calculations of important physical quantities for the gamma-ray attenuation in the B_4C (0–25 wt%) particle-reinforced Inconel 718 superalloy. The shielding properties of the B_4C (0–25 wt%) particle-reinforced Inconel 718 superalloy were studied for the first time to use not only in nuclear technology but also in other technologies such as nanotechnology and space technology.The effects of the weight percentage of the B_4C content in these superalloy materials on the gamma-ray attenuation were determined. The LAC, MAC, EBF,TVL, HVL,MFP, Z_{eff}, and FNRC values of the B_4C (0–25 wt%) particle-reinforced Inconel 718 superalloy (which contains special alloy elements such as Ni, Cr, Nb, Mo, etc.) composites were theoretically calculated for the first time to evaluate gamma and neutron radiation shielding effectiveness using the PSD software. The computed values of the MAC indicated that the decrease in the weight fraction of the B_4C compound in the Inconel 718 superalloy composites improved the attenuation performance of the materials, which could be used as shielding materials.The MFP, HVL, and TVL values were observed to increase with an increase in the gamma-ray energies and the weight fraction of the B_4C compound in the Inconel 718 superalloy composites. This was due to density and variations in the chemical composition of these superalloy materials. The higher values of MFP, HVL, and TVL imply that thicker materials are required to attenuate radiation to a safe level. Therefore, materials with lower HVL values, rather than those with higher HVL values, are desired to reduce the cost and the size. Consequently, because the Inconel 718 superalloy materials with B_4C addition have a low gamma absorption cross-section,

Fig.9. (*continued*).

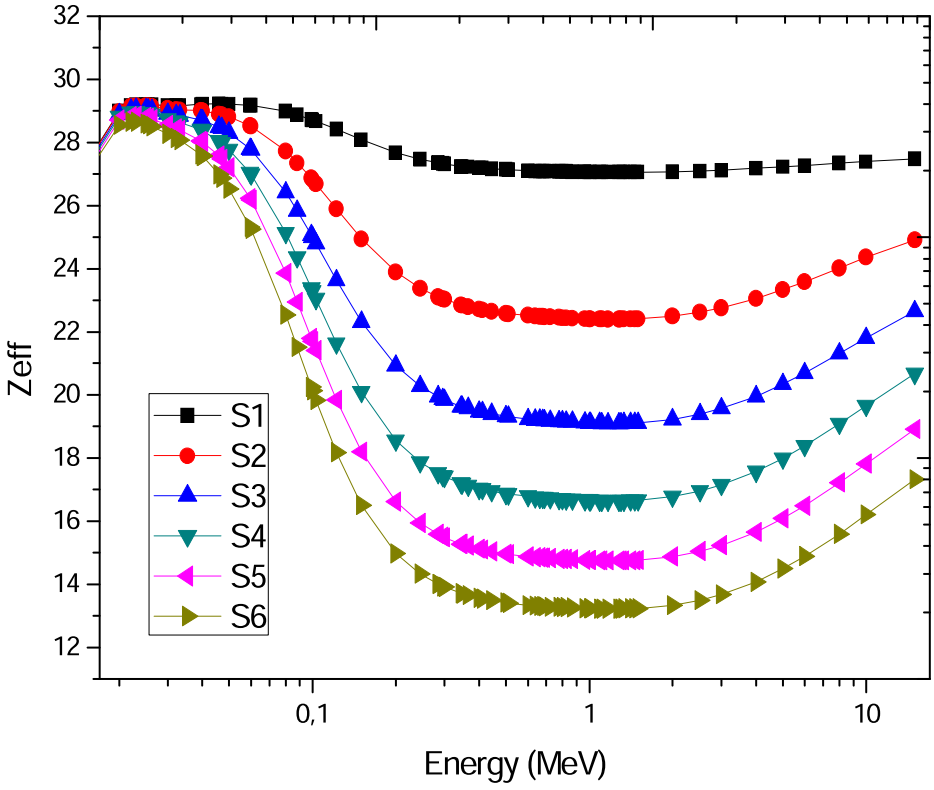

Fig. 10. Z_{eff}values calculated by Phy-X software for the S1–S6 composites.

Table 2
FNRC values of the S1–S6 composites.

	S1	S2	S3	S4	S5	S6
FNRC(1/cm)	0.159	0.169	0.177	0.183	0.189	0.194

these materials cannot absorb a wide range of gamma rays effectively. It decreases with the increase in the weight fraction of the B_4C compound in the content, thus making it an undesired material for shielding. This is because the B_4C compound's atomic number (Z) is lower than that of the Inconel superalloy. The gamma-ray attenuation capacity of the material increases with the increase in its Z value. The G-P fitting equation was used to calculate the EBF value for the photon energy range between 0.015 MeV and 15 MeV up to the penetration depth of 40 mfp. The FNRC values of these composites were calculated using the partial density method. The Inconel 718 superalloy material with B_4C (25 wt%) was found to have the highest FNRC values due to its low Z_{eff} value and low density. Therefore, the S6 (Inconel 718 superalloy material with B_4C (25 wt%) was found to be the best shielding material for neutrons. Since the choice of the shielding material and determining the required thickness of the shielding material depend on the incident gamma-ray energy, this study suggests that each quantity depends on the energy. It can be concluded that the promising properties and the fundamental parameters investigated in the present study would help utilize the involved elements in improving the shielding performance of the materials against the gamma-ray and neutron. Hence, this study is original from a variety of aspects, and its results may be used not only in nuclear technology but also in other technologies such as nano technology and space technology.

Declaration of competing interest

The authors declare that they have no known competing financial interests or personal relationships that could have appeared to influence the work reported in this paper.

Acknowledgments

The author expresses his gratitude to Gazi University Scientific Research Projects Office (Project No: GUBAP 65/2017-03) for the financial support.

Appendix A. Supplementary data

Supplementary data to this article can be found online at https://doi.org/10.1016/j.net.2021.09.028.

References

[1] D. Mengge, X. Xiangxin, He, L. Dong, W. Chao, L. Zhefu, A novel comprehensive utilization of vanadium slag: as gamma ray shielding material, J. Hazard Mater. 318 (2016) 751–757.
[2] A. Aslı, K. Esra, D. Rıdvan, Neutron and photon shielding competences of aluminum open-cell foams filled with different epoxy mixtures: an experimental study, Radiat. Phys. Chem. 182 (2021) 109382.
[3] E.R. Atta, K.M. Zakaria, A.M. Madbouly, Study on polymer clay layered nanocomposites as shielding materials for ionizing radiation, Int. J. Recent Sci. Res. 6 (2015) 4263–4264.
[4] T.A.A. Junior, M.S. Nogueira, V. Vivolo, M.P.A. Potiens, L.L. Campos, Mass attenuation coefficients of X-rays in different barite concrete used in radiation protection as shielding against ionizing radiation, Radiat. Phys. Chem. 140 (2017) 349–354.
[5] J. Kaewkhao, J. Laopaiboon, W. Chewpraditkul, Determination of effective atomic numbers and effective electron densities of Cu/Zn alloy, J. Quant. Spectrosc. Radiat. Transf. 109 (2008) 1260–1265.
[6] I. Han, L. Demir, Determination of mass attenuation coefficients, effective atomic and electron numbers for Cr, Fe, and Ni alloys at different energies, Nucl. Instrum. Methods Phys. Res. Sect. B Beam Interact. Mater. Atoms 267

(2009) 3–8.
[7] V.R.K. Murty, D.P. Winkoun, K.R.S. Devan, Effective atomic numbers for W/Cu alloy using transmission experiments, Appl. Radiat. Isot. 53 (2000) 945–948.
[8] I. Han, L. Demir, M. Sahin, Determination of mass attenuation coefficients, effective atomic and electron numbers for some natural minerals, Radiat. Phys. Chem. 78 (2009) 760–764.
[9] D. Mengge, X. Xiangxin, Y. He, L. Zhefu, Highly cost-effective shielding composite made from vanadium slag and boron-rich slag and its properties, Radiat. Phys. Chem. 141 (2017) 239–244.
[10] T. Korkut, H. Korkut, A. Karabulut, G. Budak, A new radiation shielding material: amethyst ore, Ann. Nucl. Energy 38 (2011) 56–59.
[11] J. Kaewkhao, P. Limkitjaroenporn, S. Tuscharoen, T. Kittiauchawal, W. Chewpraditkul, P. Limsuwan, Measurement of mass attenuation coefficients of blue sapphire at different photon energy by Compton scattering technique, Appl. Mech. Mater. 103 (2012) 71–75.
[12] O. Icelli, S. Erzeneoglu, M. Saglam, Effective atomic numbers of polypyrrolevia transmission method in the energy range 15.74–40.93 keV, Ann. Nucl. Energy 35 (2008) 432–437.
[13] S.R. Manohara, S.M. Hanagodimath, Effective atomic numbers for photon energy absorption of essential amino acids in the energy range 1–20 MeV, Nucl. Instrum. Methods Phys. Res. Sect. B Beam Interact. Mater. Atoms 264 (2007) 9–14.
[14] S. Erzeneoglu, O. Icelli, B. Gurbulak, A. Ates, Measurement of mass attenuation coefficients for holmium doped and undoped layered semiconductors InSe at different energies and the validity of mixture rule for crystals around the absorption edge, J. Quant. Spectrosc. Radiat. Transfer 102 (2006) 343–347.
[15] U. Cevik, H. Baltas, Measurement of the mass attenuation coefficients and electron densities for BiPbSrCaCuO superconductor at different energies, Nucl. Instrum. Methods Phys. Res. Sect. B Beam Interact. Mater. Atoms 256 (2007) 619–625.
[16] M.I. Sayyed, M.H.A. Mhareb, Y.S.M. Alajerami, K.A. Mahmoud, Imheidat Mohammad A, A. Fatimh, A. Muna, T. Al-Abdullah, Optical and radiation shielding features for a new series of borate glass samples, Optik 239 (2021) 166790.
[17] M.I. Sayyed, H.A. Aljawhara, K. Ashok, J.F.M. Jecong, I. Akkurt, Optical, mechanical properties of TeO2-CdO-PbO-B2O3 glass systems and radiation shielding investigation using EPICS2017 library, Optik 242 (2021) 167342.
[18] S. Kaewjaeng, S. Kothan, W. Chaiphaksa, N. Chanthima, R. Rajaramakrishna, H.J. Kim, J. Kaewkhao, High transparency La2O3-CaO-B2O3-SiO2 glass for diagnosis x-rays shielding material application, Radiat. Phys. Chem. 160 (2019) 41–47.
[19] H.O. Tekin, E. Kavaz, E.E. Altunsoy, O. Kilicoglu, O. Agar, T.T. Erguzel, M.I. Sayyed, An extensive investigation on gamma-ray and neutron attenuation parameters of cobalt oxide and nickel oxide substituted bioactive glasses, Ceram. Int. 45 (2019) 9934–9949.
[20] G.S. Bhandal, K. Singh, Photon attenuation coefficient and effective atomic number study of cement, Appl. Radiat. Isot. 44 (1993) 1231–1243.
[21] E. Yılmaz, H. Baltas, E. Kırıs, _I. Ustabas, U. Cevik, A.M. El-Khayatt, Gamma-ray and neutron shielding properties of some concrete materials, Ann. Nucl. Energy 38 (2011) 2204–2212.
[22] I. Akkurt, H. Akyildirim, B. Mavi, S. Kilincarslan, C. Basyigit, Gamma-ray shielding properties of concrete including barite at different energies, Prog. Nucl. Energy 52 (2010) 620–623.
[23] D. Mengge, Z. Suying, X. Xiangxin, F. Xiating, M.I. Sayyed, U. Mayeen, D.A.B. Khandaker, The potential use of boron containing resources for protection against nuclear radiation, Radiat. Phys. Chem. 188 (2021) 109601.
[24] B. Alaylar, B. Aygün, K. Turhan, G. Karadayi, S. Erdem, V.P.S. Akar, M.I. Sayyed, E. Pelit, A. Karabulut, M. Güllüce, Z. Turgut, M. Isaoglu, Characterization of gamma-ray and neutron radiation absorption properties of synthesized quinoline derivatives and their genotoxic potential, Radiat. Phys. Chem. 184 (2021) 109471.
[25] G.L. Simmons, An Adjoint Gamma-Ray Moments Computer Code, ADJMOM-I.NBS Technical Note 748, National Bureau of Standards, 1973.
[26] A.B. Chilton, C.M. Eisenhauer, G.L. Simmons, Photon point source buildup factors for air, water, and iron, Nucl. Sci. Eng. 73 (1980) 97–107.
[27] K. Takeuchi, S. Tanaka, PALLAS-ID (VII). A code for direct integration of transport equation in one-dimensional plane and spherical geometries, JAERI-M 84 (1984) 214.
[28] W.R. Nelson, H. Hirayama, D.W.O. Rogers, EGS4 Code System, SLAC-265, Stanford Linear Accelerator Centre, Stanford, California, 1985.
[29] M.I. Sayyed, Y. Elmahroug, B.O. Elbashir, A.M.I. Shams, Gamma-ray shielding properties of SLSeZnO glasses, J. Mater. Sci. Mater. Electron. (2016), https://doi.org/10.1007/s10854-016-6022-z.
[30] V.P. Singh, N.M. Badiger, Shielding efficiency of lead borate and nickel borate glasses for gamma rays and neutrons, Glass Phys. Chem. 3 (2015), 267e283.
[31] Y. Harima, Y. Sakamoto, S. Tonaka, M. Kawai, Validity of the geometric progression formula in approximating gamma-ray buildup factors, Nucl. Sci. Eng. 94 (24) (1986).
[32] ANSI/ANS-6.4.3, Gamma Ray Attenuation Coefficient and Buildup Factors for Engineering Materials, American Nuclear Society, La GrangePark, IL, USA, 1991.
[33] M. Kurudirek, Y. Ozdemir, A comprehensive study on energy absorption and exposure buildup factors for some essential amino acids and carbohydrates in the energy range 0.0015-15 MeV up to 40 mean free path, Nucl. Instrum. Methods Phys. Res. B 269 (2011) 7e19.
[34] Y. Harima, An approximation of gamma buildup factors by modified geometrical progression, Nucl. Sci. Eng. 83 (1983) 299e309.
[35] U. Kaur, J.K. Sharma, P.S. Singh, T. Singh, Comparative studies of different concretes on the basis of some photon interaction parameters, Appl. Radiat. Isot. 70 (2012) 233e240.
[36] V.P. Singh, N.M. Badiger, N. Chanthima, J. Kaewkhao, Evaluation of gamma-ray exposure buildup factors and neutron shielding for bismuth borosilicate glasses, Radiat. Phys. Chem. 98 (14e2) (1 2014).
[37] V.P. Singh, M.E. Medhat, N.M. Badiger, A.Z.M. Rahman, Radiation shielding effectiveness of newly developed superconductors, Radiat. Phys. Chem. 175e183 (2015).
[38] P.S. Singh, T. Singh, P. Kaur, Variation of energy absorption buildup factors with incident photon energy and penetration depth for some commonly used solvents, Ann. Nucl. Energy 35 (2008) 1093e1097.
[39] T. Kaur, J. Sharma, T. Singh, Review on scope of metallic alloys in gamma rays shield designing, Prog. Nucl. Energy 113 (2019) 95–113.
[40] H. Youhua, L. Yimin, H. Hao, L. Jia, T. Xiao, Preparation and mechanical properties of Inconel 718 alloy by metal injection molding, Rare Met. Mater. Eng. 39 (5) (2010) 775–780.
[41] J. Miao, T.M. Pollock, J.W. Jones, Crystallographic fatigue crack initiation in nickel-based superalloy René 88DT at elevated temperature, Acta Mater. 57 (20) (2009) 5964–5974.
[42] Y.I. Lee, N.Y. Kwon, S.T. Oh, Fabrication of Fe-base superalloy powders with yttrium oxide dispersion by mechanical alloying and chemical route, Mater. Lett. 197 (2017) 135–138.
[43] A. Suzuki, F. Wu, H. Murakami, H. Imai, High temperature characteristics of Ir–Ta coated and aluminized Ni-base single crystal superalloys, Sci. Technol. Adv. Mater. 5 (5–6) (2004) 555.
[44] A. Simchi, Densification, and microstructural evolution during co-sintering of Ni-base superalloy powders, Metall. Mater. Trans. 37 (8) (2006) 2549–2557.
[45] J.R. Hayes, J.J. Gray, A.W. Szmodis, C.A. Orme, Influence of chromium and molybdenum on the corrosion of nickel-based alloys, Corrosion 62 (6) (2006) 491–500.
[46] Z. Xu, Y. Xie, M. Ebrahimnia, H. Dang, Effect of B_4C nanoparticles on microstructure and properties of laser cladded IN625 coating, Surf. Coating. Technol. 416 (2021) 127154.
[47] O. Ozgun, H.O. Gulsoy, R. Yılmaz, F. Fındık, Microstructural and mechanical characterization of injection molded 718 superalloy powders, J. Alloys Compd. 576 (2013) 140–153.
[48] M. Xia, D. Gu, C. Ma, H. Chen, H. Zhang, Microstructure evolution, mechanical response and underlying thermodynamic mechanism of multi-phase strengthening WC/Inconel 718 composites using selective laser melting, J. Alloys Compd. 747 (2018) 684–695.
[49] A.A. Yar, M. Montazerian, H. Abdizadeh, H.R. Baharvandi, Microstructure and mechanical properties of aluminum alloy matrix composite reinforced with nano-particle MgO, J. Alloys Compd. 484 (1–2) (2009) 400–404.
[50] K. Umanath, K. Palani Kumar, S.T. Selvamani, Analysis of dry sliding wear behaviour of Al6061/SiC/Al_2O_3 hybrid metal matrix composites, Compos. B Eng. 53 (2013) 159–168.
[51] S. Karabulut, U. Gokmen, H. Cinici, Study on the mechanical and drilling properties of AA7039 composites reinforced with Al_2O_3/B_4C/SiC particles, Compos. B Eng. 93 (2016) 43–55.
[52] A. Levet, E. Kavaz, Y. Ozdemir, An experimental study on the investigation of nuclear radiation shielding characteristics in iron-boron alloys, J. Alloys Compd. 819 (2020) 152946.
[53] A. Uzun, E. Asikuzun, U. Gokmen, H. Cinici, Vickers microhardness studies on B_4C reinforced/unreinforced foamable aluminium composites, Trans. Indian Inst. Met. 71 (2) (2018) 327–337.
[54] U. Gokmen, Fabrication and characterization of hot extruded hybrid composites Al 2024 matrix reinforced with B_4C/Al_2O_3, J. Polytech. 19 (4) (2016) 445–453.
[55] B. Buyuk, A.B. Tugrul, A.C. Akarsu, A.O. Addemir, Investigation on the effects of titanium diboride particle size on radiation shielding properties of titanium diboride reinforced boron carbide–silicon carbide composites, J. Nano Electron. Phys. 4 (2012a), 01010–01013.
[56] B. Buyuk, A.B. Tugrul, A.C. Akarsu, A.O. Addemir, Investigation of behaviour of titanium diboride reinforced boron carbide–silicon carbide composites against Cs-137 gamma radioisotope source by using gamma transmission technique, Acta Phys. Pol. A 121 (2012b) 135–137.
[57] B. Buyuk, A.B. Tugrul, S. Aktop, A.O. Addemir, Investigation on the effects of boron carbide particle size on radiation shielding properties of boron carbide– titanium diboride composites, Acta Phys. Pol. A 123 (2013) 177–179.
[59] S.R. Manohara, S.M. Hanagodimath, K.S. Thind, L. Gerward, On the effective atomic number and electron density: a comprehensive set of formulas for all types of materials and energies above 1 keV, Nucl. Instrum. Methods Phys. Res., Sect. B 266 (2008) 3906–3912.
[58] Proceedings of the CAS–CERN accelerator school: beam injection, extraction and transfer, erice, Italy, 10-19 March, in: B. Holzer (Ed.), CERN Yellow Reports: School Proceedings, 5/2018, 2017. CERN-2018-008-SP (CERN, Geneva, 2018) Particle Interactions with Matter A. Lechner.
[60] A. El-Sayed, M.A.M. Ali, M.R. Ismail, Natural fibre high-density poly-ethylene and lead oxide composites for radiation shielding, Radiat. Phys. Chem. 66 (2003) 185–195.
[61] L. Gerward, N. Guilbert, K.B. Jensen, H. Levring, X-ray absorption in matter,

Reengineering XCOM. J. Radiat. Phys. Chem. 60 (2001) 23–24.
[62] L. Gerward, N. Guilbert, K.B. Jensen, H. Levring, WinXcom-a program for calculating X-ray attenuation coefficients, J. Radiat. Phys. Chem. 71 (2004) 653–654.
[63] Y. Harima, An historical review and current status of buildup factor calculations and application, Radiat. Phys. Chem. 41 (4/5) (1993) 631–672.
[64] E. Şakara, F.Ö. Özpola, B. Alım, M.I. Sayyed, M. Kurudirek, Phy-X/PSD: development of a user-friendly online software for calculation of parameters relevant to radiation shielding and dosimetry, Radiat. Phys. Chem. 166 (2020), 108496.
[65] B. Aygün, G. Budak, A new neutron absorber material: oil loaded paraffin wax, Nucl. Sci. Technol. (2012).
[66] A.B. Chilten, J.K. Shultis, R.E. Faw, Principle of Radiation Shielding, Prentice-Hall, Englewood Cliffs, N.J., 1984.
[67] M.F. Kaplan, Concrete Radiation Shielding, Longman scientific and Technology, Lonman Group UK, Limited, Essex, England., 1989.
[68] F. Akman, I. Ozkan, M.R. Kaçal, H. Polat, S.A.M. Issa, H.O. Tekin, O. Agar, Shielding features, to non-ionizing and ionizing photons, of FeCr-based composites, Appl. Radiat. Isot. (2021), https://doi.org/10.1016/j.apradiso.2020.109470.
[69] G. Kilic, S.A.M. Issa, E. Ilik, O. Kilicoglu, H.O. Tekin, A journey for exploration of Eu2O3 reinforcement effect on zinc-borate glasses: synthesis, optical, physical and nuclear radiation shielding properties, Ceram. Int. (2020), https://doi.org/10.1016/j. ceramint.2020.09.103.